Generation and Amplification of Third-Order Orbital Angular Momentum Modes in a Low-Loss All-Fiber System

Mengdi Zhang, Jianxiang Wen, Yan Wu, Ying Cao, Yanhua Luo, *Senior Member, IEEE*, Xiaobei Zhang, Fufei Pang, *Senior Member, IEEE*, Wei Chen, and Tingyun Wang

***Abstract*—We theoretically and experimentally proposed the generation method of third-order orbital angular momentum (OAM) modes with reduced losses by cascading two adiabatic mode selective couplers (MSCs), in which the LP_{11} mode produced as an excitation mode was utilized to generate a higher-order mode (LP_{31}). The minimum excess loss and insertion loss of cascaded MSCs were 3.7 dB and 5.3 dB, and had been greatly reduced compared to a single MSC. Then, the third-order OAM mode turned from LP_{31} mode was amplified in an all-fiber system, by which maximum mode gain after amplification can be achieved up to 23.2 dB. This generation and amplification system has promising applications in the long-distance mode division multiplexing technology.**

***Index Terms*—Mode selective coupler, vortex beams, higher-order mode, fiber-optics amplifiers.**

I. Introduction

With the rapid development of the modern society, single-mode fibers (SMFs) guiding only one mode have been approaching their transmission capacity limit [1]. In order to delay this capacity shortage, SMFs have gradually been replaced by few-mode fibers, which can support considerable eigenmodes transmission [2], [3]. When the degenerate modes satisfy a phase difference of $\pi/2$, a beam with orbital angular momentum (OAM) can be produced, which is called an OAM beam or an optical vortex beam [4]. Vortex beams have a spiral phase wavefront and infinite topological charge numbers, therefore having applied in many advanced fields, such as particle trapping [5], optical tweezers [6], optical sensor [7], photon entanglement [8]. underwater wireless optical communication [9] and optical fiber communication [10]. At present, there are two mainly generation methods of OAM modes, free space-based and optical fiber-based methods, including spatial light modulators [11], [12], fiber gratings [13], [14], helical long-period fiber grating [15], [16] and mode selective couplers (MSCs) [17], [18], [19], [20], [21]. Among these methods, MSC can be considered valuable due to the virtue of low loss, small size, and easy to couple with fibers. However, traditional MSCs can generate the higher-order modes directly only from the fundamental mode, resulting in high losses that is not conductive to the development of optical communication.

In this article, we demonstrated an all-fiber excitation method of third-order modes via cascaded adiabatic MSCs, from which this cascade system enables decreased losses. Then, we realized amplification of the third-order OAM mode generated by low-loss cascaded couplers.

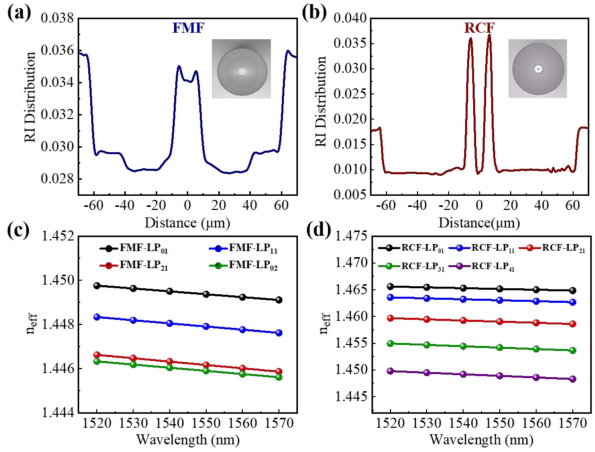

Fig. 1. Refractive index distribution of (a) FMF and (b) RCF (Insets: fiber cross sections). Variation of n_{eff} distribution versus wavelength of (c) FMF and (d) RCF.

II. Fiber Parameters

The optical fibers we used in the experiment include SMF (Corning SMF-28e fiber), four-mode fiber (FMF), and ring-core fiber (RCF) [21]. Fig. 1(a) and (b) show the cross sections and refractive index (RI) profiles of the FMF and RCF. The geometrical parameters of the two fibers are as follows. For FMF, $D_{core} = 17.0\ \mu m$, $D_{cladding} = 125.0\ \mu m$, and the RI

Manuscript received 7 June 2023; revised 2 August 2023; accepted 26 August 2023. Date of publication 30 August 2023; date of current version 8 September 2023. This work was supported in part by the National Natural Science Foundation of China under Grants 61975113 and 61935002, in part by the Shanghai Professional Technical Public Service Platform of Advanced Optical Waveguide Intelligent Manufacturing and Testing under Grant 19DZ2294000, and in part by the 111 Project under Grant D20031. *(Corresponding author: Jianxiang Wen.)*

The authors are with the Key Laboratory of Specialty Fiber Optics and Optical Access Networks, Joint International Research Laboratory of Specialty Fiber Optics and Advanced Communication, Shanghai Institute for Advanced Communication and Data Science, Shanghai University, Shanghai 200444, China (e-mail: 1128@shu.edu.cn; wenjx@shu.edu.cn; wuyan0604@shu.edu.cn; cao0827@shu.edu.cn; yhluo3@shu.edu.cn; xbzhang@shu.edu.cn; ffpang@shu.edu.cn; chenweisd@shu.edu.cn; tywang@shu.edu.cn).

Digital Object Identifier 10.1109/JPHOT.2023.3310210

difference between the core and cladding layer is ∼0.006. For RCF, $D_{core} = 6.5\ \mu m$, $D_{ring} = 18.0\ \mu m$, $D_{cladding} = 125.0\ \mu m$, and the ring-shaped structure enables the RI difference between the ring and cladding layer of 0.027.

According to the fiber parameters of the FMF and RCF, the mode effective refractive index (n_{eff}) was simulated by the method of finite element analysis (COMSOL Multiphysics software), as shown in Fig. 1(c) and (d). Note that FMF can support LP_{01}, LP_{11}, LP_{21}, and LP_{02} modes and RCF can support LP_{01}, LP_{11}, LP_{21}, LP_{31}, and LP_{41} mode. The n_{eff} difference between different order modes are more than 10^{-4} in the two optical fibers [22], which can effectively avoid the crosstalk between different order modes to produce and transmit stable OAM modes.

III. Generation of LP_{31} Mode in MSC

The principle of the MSC is closely following the coupled mode theory [23]. The precondition of efficient coupling is the same n_{eff}. Its content is that if the optical fiber coupling system only consists of two fibers, we can get the coupling model equation as:

$$\frac{dA}{dz} + i\beta_A A(z) = -ik_{AB}B(z) \tag{1}$$

$$\frac{dB}{dz} + i\beta_B B(z) = -ik_{BA}A(z) \tag{2}$$

Where A and B are the excited mode amplitudes in each fiber, respectively; β_A and β_B are the propagation constants of excited modes in two fibers, k_{AB} and k_{BA} are the coupling coefficients and $k_{AB} \approx k_{BA} = k$, which depends on the cross-section geometry and index profile of the fibers. We assumed $\beta_A = \beta_B = \beta$, which means the phase mismatch is zero, $a(z) = A(z)e^{i\beta_A z}$, and $b(z) = B(z)e^{i\beta_B z}$. After a detailed calculation and analysis, the status of power between two fibers can be expressed as:

$$P_A = |A(z)|^2 = \cos^2(kz) \tag{3}$$

$$P_B = |B(z)|^2 = \sin^2(kz) \tag{4}$$

Where P_A and P_B are the output power of fiber A and fiber B, respectively. From the equations above, we notice that the power presents a complete periodic transfer and can be fully converted between two fibers.

Based on the coupled mode theory and the fused taper method [24], we fabricated a MSC by utilizing the SMF and RCF under adiabatic conditions [25]. The relationship between n_{eff} of different-order modes in the SMF and RCF as a function of fiber radius was investigated, as shown in Fig. 2(a). It can be seen that for LP_{31} mode generation, the modes have the same value of n_{eff} with a scaling factor $\rho = R_{SMF}/R_{RCF} = 3.1/6.4 = 0.48$. Thus, the SMF needed to be pre-stretched with a diameter of 60.0 μm. The experimental pre-stretched diameter of the SMF was ∼62.4 μm. Furthermore, the mode conversion process along the coupler was simulated using a beam propagation method in the commercial simulation software (RSoft), whose results are shown in Fig. 2(b). The mode conversion from LP_{01} to LP_{31} mode can be illustrated that (I) LP_{01} mode was launched into the SMF; (II) The cladding layers of the two fibers gradually

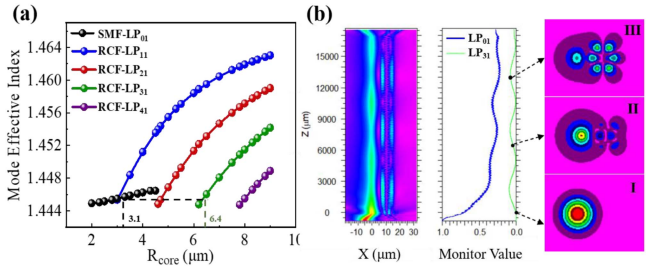

Fig. 2. (a) n_{eff} of different modes in SMF and RCF as a function of fiber core radius. (b) Mode conversion process between the LP_{01} in the SMF and the LP_{31} mode in the RCF along the coupler.

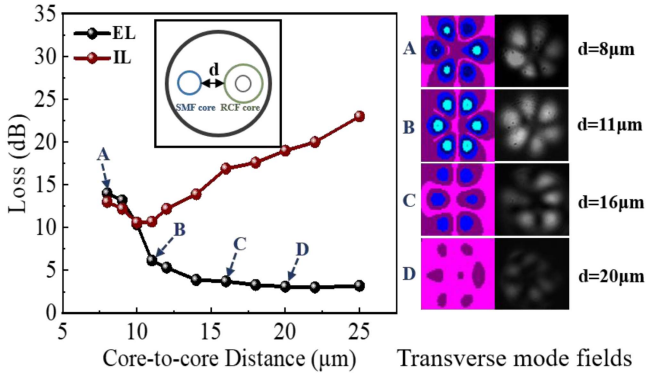

Fig. 3. Variation of losses and transverse mode patterns at positions 'A', 'B', 'C', and 'D' with different *d* (inset: cross section of coupling region of MSC).

merged along the coupling region, and the energy between the LP_{01} mode in the SMF and the LP_{31} mode in the RCF proceeded back and forth periodically with the increase of transmission distance; (III) LP_{31} mode can be excited in the MSC.

One of the most important parameters of fiber coupler is loss, which includes losses, excess loss (EL) and insertion loss (IL). The losses refer to the general term for excess loss (EL) and insertion loss (IL), while the lowest losses represent the relatively minimum sum of EL and IL of fiber coupler. EL and IL can be calculated using the following equations:

$$EL = 10\lg\frac{P_{in}}{\sum P_{out}} \tag{5}$$

$$IL = 10\lg\frac{P_{in}}{P_{outl}} \tag{6}$$

where P_{in}, ΣP_{out} and P_{outl} denote the input power, the total output power and high-order mode output power of fiber coupler. *l* is the order of OAM mode, which can be taken as 1, 2 and 3.

There are many factors that affect the losses of couplers during the taper process, such as fiber geometry structure, stretching length, and core-to-core distance (marked as '*d*'). The influence of *d* directly determined the degree of coupling between modes in two fibers. Then, we will discuss how to reduce the losses of couplers from this parameter. Subsequently, we explored the losses, EL and IL, of the MSC with varying the *d* between the SMF and RCF cores [26], as shown in Fig. 3. Four different *d* values 8.0, 11.0, 16.0, and 20.0 μm were elaborated, in which the simulated and experimental transverse mode fields were exhibited as 'A', 'B', 'C', and 'D'.

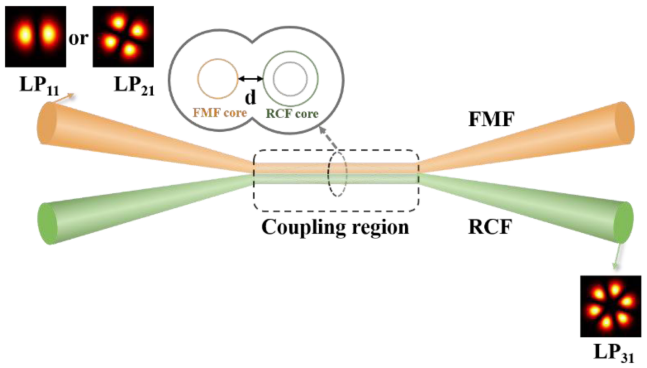

Fig. 4. Modeling of the MSC. When a high-order mode was launched into the FMF, a LP_{31} mode can be generated.

In the simulation, EL is ∼6.0 dB and IL is ∼10.0 dB, while experimentally EL is ∼8.5 dB and IL is ∼11.3 dB with the d of 11.0 μm. The decreasing trend in EL before $d = 14.0$ μm is attributed to the fact that the d is too small to mode crosstalk. As the d value increases, more LP_{01} modes couple into LP_{31} mode until $d = 14.0$ μm, then the EL becomes small and remains almost unchanged because LP_{01} mode is difficult to convert into LP_{31} mode. As a result, the power of the LP_{01} mode increases while the power of the LP_{31} mode decreases. At this point, the total power of the LP_{01} and LP_{31} modes output from the coupler remains comparatively unchanged, resulting in a relatively stable EL. As for IL, it is commonly used to characterize coupling efficiency. The mode crosstalk before $d = 11.0$ μm leads to a little output power of the LP_{31} mode and low coupling efficiency. As d value increases, the likelihood of LP_{01} coupling into LP_{31} increases. However, the coupling becomes weaker after $d = 11.0$ μm, while the output power of the LP_{31} mode sharply decreases, leading to a decrease in coupling efficiency and impacting the IL trend. Under consideration of factors, it is recommended to choose parameter of $d = 11.0$ μm for fabricating the coupler. However, the losses of MSC for its forward applications are still too large to use. Therefore, higher-order mode generation with cascading two couplers is adopted to solve this problem.

IV. Generation of Third-Order OAM Mode in Cascaded MSCs

For the above-mentioned LP_{31}-mode MSC, which is directly excited by LP_{01} and drawn by SMF and RCF, has a significant difference in core size between two fibers. In order to achieve a complete conversion process by matching the same n_{eff} between LP_{01} in SMF and LP_{31} in RCF, it is required to set the pre-stretched length of SMF to a large value, which leads to a smaller size SMF and increased mode leakage, resulting in excessive losses of the MSC and difficulty in generating higher-order modes. Accordingly, we altered the input mode of MSC from fundamental mode to the lower-order modes as the excitation mode to generate LP_{31} to reduce the pre-stretched length and minimize energy leakage, as shown in Fig. 4. At the same time, we had also replaced SMF with FMF that can transmit high-order modes to fabricate MSCs with RCF that can

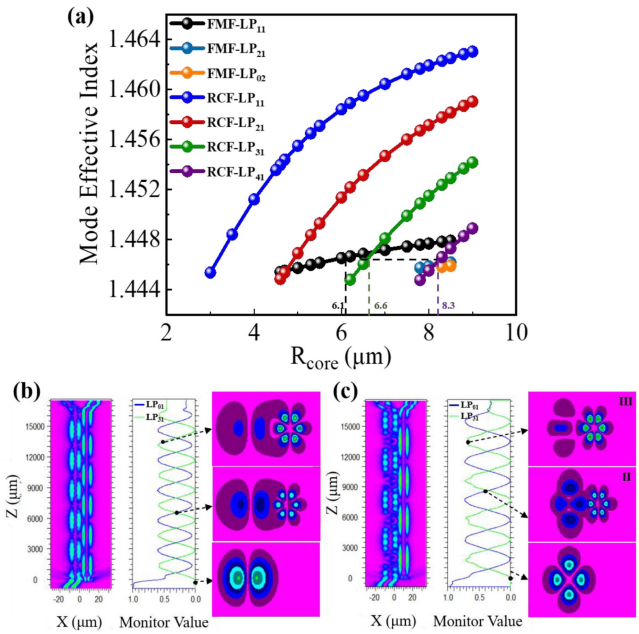

Fig. 5. (a) n_{eff} of different modes of FMF and RCF as a function of fiber core radius. Mode conversion process between the (b) LP_{11} and (c) LP_{21} modes in the FMF and the LP_{31} mode in the RCF along the couplers.

be used to address the issue of low-loss and higher-order modes in all-fiber systems.

Here we considered LP_{11} and LP_{21} modes as the input modes and investigated the performance of the mode conversion. Firstly, we fabricated a MSC1 with the SMF and FMF to excite high-order modes, i.e., LP_{11} and LP_{21} modes. Then, FMF and RCF were used to manufacture MSC2. Fig. 5(a) shows the relationship between the n_{eff} of each mode of FMF and RCF as a function of the fiber radius. It can be seen that when the LP_{11} mode of FMF and the LP_{31} mode of RCF have the same n_{eff} to meet the mode conversion, in which the scaling factor $\rho = R_{FMF}/R_{RCF} = 6.1/6.6 = \sim 0.92$. At this time, the FMF only needs to be pre-stretched as a diameter of 115 μm, which can perform mode conversion with RCF to generate LP_{31} mode. Similarly, when the scaling factor $\rho = R_{RCF}/R_{FMF} = 6.6/8.3 = \sim 0.78$, LP_{31} mode can be generated from LP_{21} mode. The fabrication of coupler has satisfied adiabatic conditions as discussed previously. We simulated the energy conversion and mode coupling between the LP_{11}/LP_{21} mode in FMF and the LP_{31} mode in RCF, as shown in Fig. 5(b) and (c), respectively. Compared with Fig. 2(b), higher conversion efficiency and higher output power of LP_{31} mode were realized in these processes.

Similarly, the losses of MSC2s generated from LP_{11} and LP_{21} modes were analyzed with different d values, as shown in Fig. 6(a) and (b) respectively. The same tendency of losses as that in Fig. 3 were obtained. We consider that when d decreases, it will cause strong coupling effect, leading to crosstalk between the lower-order mode in FMF and the high-order mode in RCF, resulting in increasing losses. At the same time, decrease in d also means that the diameter of the fiber should be smaller, which will cause more energy leakage in high-order modes.

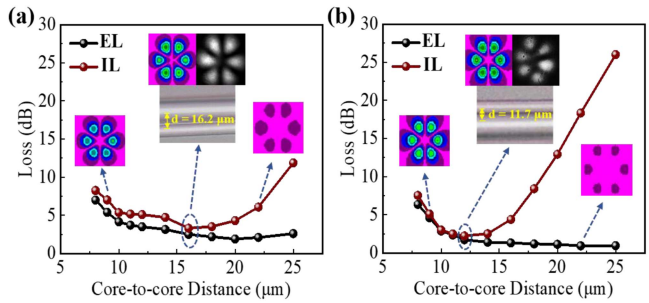

Fig. 6. Losses of third-order mode couplers excited by (a) LP_{11} and (b) LP_{21} as a function of the core-to-core distance.

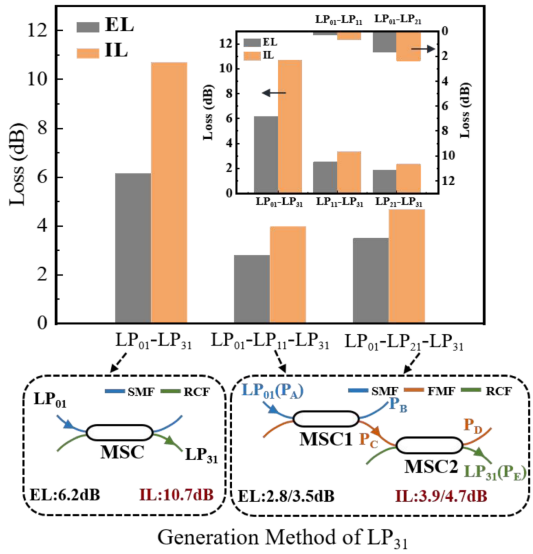

Fig. 7. Losses characteristics of single MSC and cascaded MSCs.

When d increases, the lower-order modes in FMF enter the cladding, and are difficult to couple into the core of RCF to convert into high-order modes, resulting in increasing losses. However, the IL of the LP_{31}-mode MSC2 excited by the LP_{21} mode rapidly increased after $d = 14.0$ μm, which is higher and steeper compared to MSC2 excited by the LP_{11} mode, as brown line shown in Fig. 6(b). This indicates that MSC2 excited by LP_{21} is highly sensitive to variations in fiber structure and exhibits a stronger dependence on d. Additionally, in Fig. 6(a), three specific d values 9.0, 16.0, and 22.0 μm were demonstrated to observe the transverse mode fields of LP_{31} mode excited by LP_{11}. The optimal d with relatively low losses was 16.0 μm, while experimental d value was $\sim$16.2 μm. Likewise, in Fig. 6(b), the LP_{31} mode excited by LP_{21} with d values 9.0, 16.0, and 22.0 μm were explored, where 12.0 μm was optimal, and the experimental value was $\sim$11.7 μm.

We then summarized the losses of different mode generation methods with optimal d values, and provided the models of single MSC and cascaded MSCs, as shown in Fig. 7. In model of cascaded MSCs, P_A represents the input power of LP_{01} mode, P_C represents the output power of lower-order modes in MSC1, and P_E represents the final output power of LP_{31} mode.

When the LP_{31} mode was directly generated from LP_{01} mode, EL and IL were respectively 6.2 dB and 10.7 dB. When

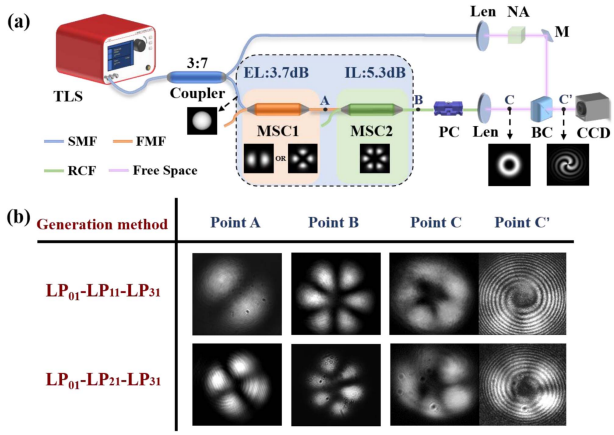

Fig. 8. (a) Schematic of the experimental setup for generating and detecting high-order mode in the MSCs. (b) Experimentally recorded transverse mode fields and interference patterns.

high-order modes, LP_{11} and LP_{21} modes, were used to excite LP_{31} mode, EL were 2.8 dB and 3.5 dB, as well as IL were 3.9 dB and 4.7 dB, as shown in Fig. 7. The losses corresponding to MSC1 and MSC2 in cascading are shown in the insert of Fig. 7. Due to the high losses when MSC1 generated LP_{21}, the loss when using LP_{11}-mode MSC1 to excite MSC2 to generate LP_{31} with cascaded method is relatively small. Therefore, cascaded MSCs with LP_{11} mode excitation can realize the minimum losses.

We established an all-fiber third-order OAM mode generation system, which was mainly composed of a MSC1, a MSC2, and a real-time monitoring system, as shown in Fig. 8(a). A tunable laser (TLS, Santec TSL-710) was used as a signal light, whose wavelength range was from 1480 nm to 1640 nm. The signal light was divided by a coupler with the optical splitter of 3:7 into two paths. One path was used for a reference beam; the other path was connected to the MSC1-fabricated with the SMF and FMF - that converted the fundamental mode into LP_{11} or LP_{21} modes. Then, it was launched with the MSC2 fabricated with the FMF and RCF - that converted the input lower-order mode into a higher-order mode, LP_{31} mode. The pulling rate before coupling, after coupling and the correction stage were set to 100-150 μm/s, 40-70 μm/s and 10-30 μm/s. According to the simulation results, the pulling length of MSC2 were set to approximately 17973 and 20648 μm while injecting LP_{11} mode or LP_{21} mode. The polarization controller (PC) was employed to tune the polarization state of the output mode from LP_{31} mode to the third-order OAM mode. The character 'M' referred to a reflection mirror. The higher-order mode and the reference beam were combined by a beam combiner (BC). A neutral attenuator (NA) can balance the power of beam in both, channels and a charge-coupled device (CCD, HAMAMATSUC10633) camera was used to observe the transverse mode fields and the corresponding interference patterns.

The observation results at positions 'A', 'B', 'C', and 'C" are shown in Fig. 8(b). It can be seen that the third-order OAM can be generated by cascading two MSCs. When the output of MSC1 was LP_{11} mode (EL = 0.6 dB, IL = 1.7 dB), the overall

TABLE I
PERFORMANCE COMPARISON OF OAM MODES GENERATION IN MSCS

Order of OAM	EL (dB)	IL (dB)	Scaling factor	Purity (%)	Ref.
1st	—	1.2	0.63	72	[17]
1st/2nd	0.4/2.5	—	0.68/0.40	—	[18]
1st/2nd	—	1.3/3.1	—	—	[19]
2nd	3.5	4.1	0.45	—	[20]
1st/2nd/3rd	1.0/5.0/9.0	1.7/5.6/10.1	0.94/0.66/0.54	—	[21]
3rd	6.2[a]/8.5[b]	10.7[a]/11.3[b]	0.48[a]/0.50[b]	51	This work
3rd	2.8[a]/3.7[b]	3.9[a]/5.3[b]	0.92[a]/0.89[b]	92	This work[c]

[a] Simulation; [b] Experiment; [c] Cascading MSCs.

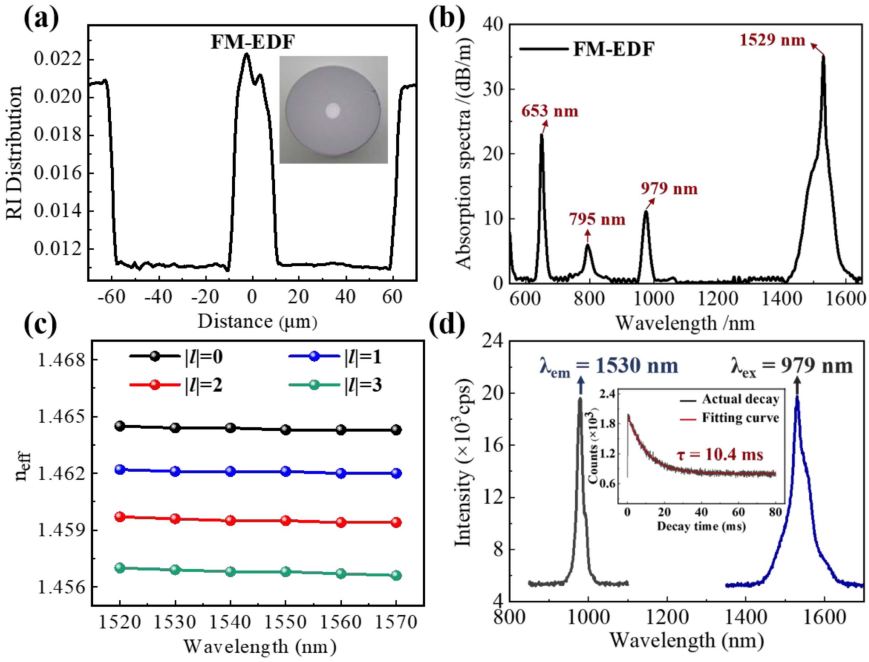

Fig. 9. Performance parameter of FM-EDF: (a) refraction index distribution and the cross-sectional image (inset), (b) absorption spectrum, (c) simulated n_{eff} as a function of the wavelength, and (d) excitation-emission spectra and fluorescence decay curves (inset).

EL and IL of the cascaded couplers were 3.7 dB and 5.3 dB at the d of MSC2 of ~16.2 μm. When MSC1 output LP_{21} mode (EL = 2.6 dB, IL = 3.5 dB), the overall EL and IL were 5.4 dB and 6.3 dB, and the d of the MSC2 was ~11.7 μm. Moreover, we summarized the performance of several OAM mode generation methods based on MSCs, as illustrated in Table I. Relatively lower losses can be obtained for the lower-order OAM modes, whereas the higher losses occurred in the generated third-order OAM modes. In other work, the EL and IL of the third-order OAM modes were as high as 9.0 dB and 10.1 dB, respectively. On the contrary, cascading MSCs proposed in this work can effectively reduce losses to 3.7 dB and 5.3 dB. And the purity of the third-order OAM mode excited by LP_{11} at wavelength 1550 nm was up to ~89%.

Fig. 9(a) shows the refractive index distribution and cross-section image of the FM-EDF. The core and cladding diameters are 20.6 μm and 125.0 μm, respectively. The refractive index difference between the core and cladding layer is approximately 0.011. Fig. 9(b) shows the absorption spectrum, in which four typical absorption peaks of Er ion exist at 653 nm, 795 nm, 979 nm, and 1529 nm. Especially the absorption coefficient can reach 11.1 dB/m at 979 nm. According to the fiber parameters, the effective mode refractive index (n_{eff}) of each mode in the FM-EDF was simulated, as shown in Fig. 9(c). It should be noted that in theory the FM-EDF are able to support up to 14 vortex modes, i.e., $|l| = 3$, for data transmission respectively. In addition, the excitation-emission spectra of the FM-EDF are shown in Fig. 9(d), where the excitation and emission peaks are located at 979 nm and 1530 nm, respectively. The fluorescence lifetime of erbium ions on FM-EDF is 10.4 ms under 980 nm excitation.

Fig. 10 is a diagram of an all-fiber OAM amplification system. TLS provides signal light with wavelengths ranging from 1520 nm to 1570 nm, taking a wavelength every 5 nm interval; Wherein MSC1 and MSC2 were excited in parallel to generate a third order OAM as an amplification mode; The output power of the 980 nm laser exceeds 1 W to provide sufficient pump power for the amplification system. Few-mode wavelength division multiplexer (FM-WDM) fabricated with few-mode optical fiber; which combines the OAM pump and signal into the few-mode

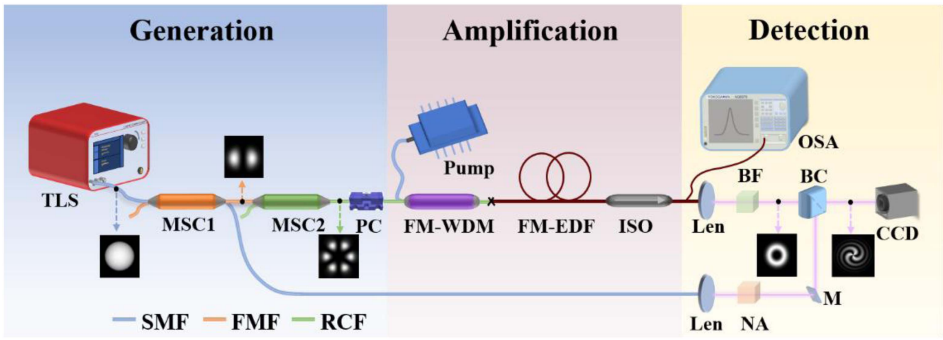

Fig. 10. Schematic diagram of all-fiber vortex amplification system.

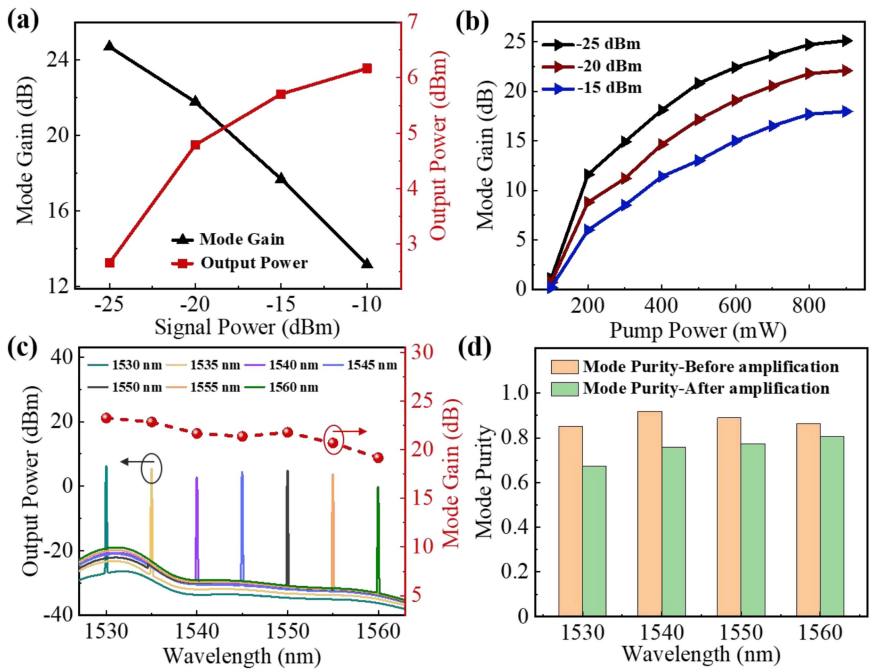

Fig. 11. Measured results of the third-order OAM amplification: (a) mode gain and output power as a function of signal power at wavelength of 1550 nm, (b) mode gain as a function of pump power at a signal wavelength of 1550 nm, (c) output power and mode gain as a function of wavelength over the C-band, and (d) mode purity as a function of wavelength.

erbium doped fiber (FM-EDF) with the length of 1.4 m. Band-pass optical filter (BF, Thorlabs FB1550-12, FWHM = 12 nm) was employed to filter out the narrow-band beam and reduce the amplified spontaneous emission (ASE) effect. And FM-WDM fabricated with the homemade RCF can maintain the OAM mode transmission. The isolator (ISO) in the measurement system was used to prevent laser oscillation and protect the optical spectrum analyzer (OSA, Yokogawa AQ6370D, Japan). The center wavelength and bandwidth range of the isolator were approximately 1310 nm and ±30 nm.

Here, the output power and mode gain as a function of input signal power at 1550 nm were measured, as shown in Fig. 11(a), and the maximum mode gain and maximum output power were measured as 24.7 dB and 6.2 dBm. Moreover, the mode gain versus the pump power for the third-order OAM mode was depicted in Fig. 11(b). With increasing the pump power, the mode gain increased and tended to saturate at 800 mW, which the saturation value became higher with increasing the signal power. The recorded mode gain and output power of the third-order OAM mode after amplification are shown in Fig. 11(c). The mode gains of third-order OAM mode were beyond 19.1 dB over the C-band, which the power of the signal light and the pump power are fixed at −20 dBm and 800 mW. And the maximum output power is 6.3 dB at the wavelength of 1530 nm under the pump light with the power of 800 mW. Based on the calculation method for the first-order OAM mode purity proposed by N. Bozinovic [27], The mode purity of third-order OAM mode before and after amplification at different wavelength is calculated by adding the left-handed and right-handed components in the third-order OAM mode, as shown in Fig. 11(d). The third-order OAM mode purity before amplification with an average mode purity of 87%. The mode purity of the third-order OAM mode after amplification was slightly reduced with an average mode purity of 74%.

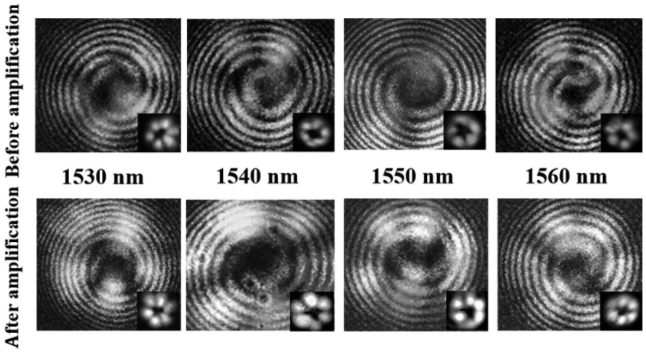

Fig. 12. Helical interference fringes and transverse mode fields of the third-order OAM before and after amplification.

Then, we took out some point sites at different wavelengths (1530, 1550, 1560, and 1570 nm) from the spectrum, as shown in Fig. 12, and observed helical interference fringes of third-order OAM before and after amplification. This method to generate and amplify higher-order OAM modes could be applied in long-haul optical fiber communication systems in the future.

V. Conclusion

We employed MSC1 fabricated with SMF and FMF that can generate LP_{11} or LP_{21} mode as an excitation mode, which was further injected into MSC2 fabricated with FMF and RCF to produce LP_{31} mode. The conversion process and power variation of the higher-order mode were accomplished theoretically and experimentally. The experiment results show that the minimum EL and IL obtained in a single MSC system were ∼8.5 dB and 11.3 dB, whereas those in cascaded MSCs system were ∼3.7 dB and 5.3 dB. Therefore, compared with traditional MSC, cascaded MSCs can realize desirable performance of low loss and handy fabrication. Furthermore, we tuned LP_{31} mode to the third-order OAM modes and thus established an OAM amplification system. The high mode purity can be completed, in which maximum mode gain and purity could reach 23.2 dB and 81%. This method to generate and amplify higher-order OAM modes can be widely applied in long-distance mode division multiplexing technology.

References

[1] R. J. Essiambre, G. Kramer, P. J. Winzer, G. J. Foschini, and B. Goebel, "Capacity limits of optical fiber networks," *J. Lightw. Technol.*, vol. 28, no. 4, pp. 662–701, Feb. 2010, doi: 10.1109/JLT.2009.2039464.

[2] D. Mao et al., "Generation of polarization and phase singular beams in fibers and fiber lasers," *Adv. Photon.*, vol. 3, no. 1, Jan. 2021, Art. no. 014002, doi: 10.1117/1. AP. 3.1.014002.

[3] Y. Lian, Y. Yu, S. Han, N. Luan, Y. Wang, and Z. Lu, "OAM Beams generation technology in optical fiber: A review," *IEEE Sens. J.*, vol. 22, no. 5, pp. 3828–3843, Mar. 2022, doi: 10.1109/JSEN.2022.3145833.

[4] Y. Bai, H. Lv, X. Fu, and Y. Yang, "Vortex beam: Generation and detection of orbital angular momentum," *Chin. Opt. Lett.*, vol. 20, no. 1, Jan. 2022, Art. no. 012601, doi: 10.3788/COL202220.012601.

[5] H. Kawauchi, K. Yonezawa, Y. Kozawa, and S. Sato, "Calculation of optical trapping forces on a dielectric sphere in the ray optics regime produced by a radially polarized laser beam," *Opt. Lett.*, vol. 32, no. 13, pp. 1839–1841, Jul. 2007, doi: 10.1364/OL.32.001839.

[6] M. Padgett and R. Bowman, "Tweezers with a twist," *Nature Photon.*, vol. 5, no. 6, pp. 343–348, Jun. 2011, doi: 10.1038/NPHOTON.2011.81.

[7] X. Fu et al., "Seven-core fiber torsion sensor with microcavity structure based on intensity measurement," *Opt. Commun.*, vol. 502, Sep. 2021, Art. no. 127412, doi: 10.1016/j.optcom.2021.127412.

[8] S. Franke-Arnold, L. Allen, and M. Padgett, "Advances in optical angular momentum," *Laser Photon. Rev.*, vol. 2, no. 4, pp. 299–313, Aug. 2008, doi: 10.1002/lpor.200810007.

[9] L. Zhu et al., "Adaptive optics for orbital angular momentum-based Internet of Underwater Things applications," *IEEE Internet Thing J.*, vol. 9, no. 23, pp. 24281–24299, Dec. 2022, doi: 10.1109/JIOT.2022.3190268.

[10] S. Zhou, X. Liu, R. Gao, Z. Jiang, H. Zhang, and X. Xin, "Adaptive Bayesian neural networks nonlinear equalizer in a 300-gbit/s PAM8 transmission for IM/DD OAM mode division multiplexing," *Opt. Lett.*, vol. 48, no. 2, pp. 464–467, May 2023, doi: 10.1364/OL.480532.

[11] Y. Xie, Y. Yang, L. Han, Q. Yue, and C. Guo, "Generation of arbitrary vector beams based on a single spatial light modulator and a thin-film polarization splitting cubic," *Chin. Opt. Lett.*, vol. 14, no. 12, Dec. 2017, Art. no. 122601, doi: 10.3788/COL201614.122601.

[12] Z. Zhao et al., "Division and multiplication of the state order for data-carrying orbital angular momentum beams," *APL Photon.*, vol. 1, no. 9, Dec. 2016, Art. no. 090802, doi: 10.1063/1.4968838.

[13] K. Yang et al., "Femtosecond laser inscription of fiber Bragg grating in twin-core few-mode fiber for directional bend sensing," *J. Lightw. Technol.*, vol. 35, no. 21, pp. 4670–4676, Nov. 2017, doi: 10.1109/JLT.2017.2750407.

[14] Y. Zhao, M. Tang, Y. Ma, Y. Liu, Y. Yang, and Z. He, "Fabrication and sensing characteristics of long-period fiber grating in capillary fiber," *IEEE Sens. J.*, vol. 23, no. 4, pp. 3581–3588, Feb. 2023, doi: 10.1109/JSEN.2022.3226743.

[15] T. Detani, H. Zhao, P. Wang, T. Suzuki, and H. Li, "Simultaneous generation of the second- and third-order OAM modes by using a high-order helical long-period fiber grating," *Opt. Lett.*, vol. 46, no. 5, pp. 949–952, Mar. 2021, doi: 10.1364/OL.418248.

[16] W. Chang, M. Feng, B. Mao, P. Wang, Z. Wang, and Y. G. Liu, "All-fiber fourth-order OAM mode generation employing a long period fiber grating written by preset twist," *J. Lightw. Technol.*, vol. 40, no. 14, pp. 4804–4811, Jul. 2022, doi: 10.1109/JLT.2022.3165708.

[17] S. Pidishety, S. Pachava, P. Gregg, S. Ramachandran, G. Brambilla, and B. Srinivasan, "Orbital angular momentum beam excitation using an all-fiber weakly fused mode selective coupler," *Opt. Lett.*, vol. 42, no. 21, pp. 4347–4350, Nov. 2017, doi: 10.1364/OL.42.004347.

[18] T. Wang et al., "Generation of femtosecond optical vortex beams in all-fiber mode-locked fiber laser using mode selective coupler," *J. Lightw. Technol.*, vol. 35, no. 11, pp. 2161–2166, Jun. 2017, doi: 10.1109/JLT.2017.2676241.

[19] Y. Huang et al., "High-order mode Yb-doped fiber lasers based on mode-selective couplers," *Opt. Exp.*, vol. 26, no. 15, pp. 19171–19181, Jun. 2018, doi: 10.1364/OE.26.019171.

[20] J. Yang et al., "All-Fiber multiplexing and transmission of high-order circularly polarized orbital angular momentum modes with mode selective couplers," *IEEE Photon J.*, vol. 11, no. 3, Jun. 2019, Art. no. 7202909, doi: 10.1109/JPHOT.2019.2910847.

[21] Y. Wu, J. Wen, F. Pang, X. Zeng, and T. Wang, "Generation of controllable high-order modes in mode selective coupler," in *Proc. IEEE 6th Optoelectron. Glob. Conf.*, 2021, pp. 124–127, doi: 10.1109/0GC52961.2021.9654426.

[22] S. Ramachandran and P. Kristensen, "Optical vortices in fiber," *Nanophotonics*, vol. 2, no. 5/6, pp. 455–474, Jan. 2013, doi: 10.1515/nanoph-2013-0047.

[23] W. Huang, "Coupled-mode theory for optical waveguides: An overview," *J. Opt. Soc. Amer. A*, vol. 11, no. 3, pp. 963–983, Mar. 1994.

[24] H. Yao et al., "A mode generator and multiplexer at visible wavelength based on all-fiber mode selective coupler," *Nanophotonics*, vol. 9, no. 4, pp. 973–981, Apr. 2020, doi: 10.1515/nanoph-2020-0050.

[25] D. Mao et al., "Adiabatic coupler with nonlinearly tapered mode-evolution region," *IEEE Photon. Technol. Lett.*, vol. 33, no. 16, pp. 840–843, Aug. 2021, doi: 10.1109/LPT.2021.3072787.

[26] Z. Zhang et al., "Low-crosstalk orbital angular momentum fiber coupler design," *Opt. Exp.*, vol. 25, no. 10, pp. 11200–11209, May 2017, doi: 10.1364/OE.25.011200.

[27] N. Bozinovic, S. Golowich, P. Kristensen, and S. Ramachandran, "Control of orbital angular momentum of light with optical fibers," *Opt. Lett.*, vol. 37, no. 13, pp. 2451–2453, Jul. 2012, doi: 10.1364/OL.37.002451.